Nuclear Instruments and Methods in Physics Research A 710 (2013) 82–86

Contents lists available at SciVerse ScienceDirect

Nuclear Instruments and Methods in Physics Research A

journal homepage: www.elsevier.com/locate/nima

In situ fine tuning of bendable soft x-ray mirrors using a lateral shearing interferometer

Daniel J. Merthe [a], Kenneth A. Goldberg [b], Valeriy V. Yashchuk [a,*], Wayne R. McKinney [a], Richard Celestre [a], Iacopo Mochi [b], James MacDougall [b], Gregory Y. Morrison [c], Senajith B. Rekawa [c], Erik Anderson [c], Brian V. Smith [c], Edward E. Domning [c], Howard Padmore [a]

[a] Advanced Light Source, Lawrence Berkeley National Laboratory, Berkeley, USA
[b] Center for X-Ray Optics, Lawrence Berkeley National Laboratory, Berkeley, USA
[c] Engineering Division, Lawrence Berkeley National Laboratory, Berkeley, USA

ARTICLE INFO

Available online 12 November 2012

Keywords:
Metrology of x-ray optics
Synchrotron radiation
Shearing interferometry
Knife-edge measurement

ABSTRACT

Broadly applicable, in situ at-wavelength metrology methods for x-ray optics are currently under development at the Advanced Light Source. We demonstrate the use of quantitative wavefront feedback from a lateral shearing interferometer for the suppression of aberrations. With the high sensitivity provided by the interferometer we were able to optimally tune the bending couples of a single elliptical mirror (NA=2.7 mrad) in order to focus a beam of soft x-rays (1.24 keV) to a nearly diffraction-limited beam waist size of 156($\pm$10) nm.

1. Introduction

Current and next generation synchrotron light sources are pushing the limits of resolution in order to probe interesting natural and man-made materials. This requires the development of high throughput x-ray optics capable of maintaining diffraction-limited focusing performance. Despite the recent advances in fabrication and state-of-the-art ex situ metrology, beamline optics degrade over time due to use, temperature variations, and mechanical instabilities. For this reason we at the Advanced Light Source (ALS) and other groups [1–11] are developing comprehensive at-wavelength techniques for in situ characterization and optimization of x-ray optics.

We present here a technique for optimally tuning the bending couples of a deformable focusing mirror in situ, using quantitative wavefront feedback from a lateral shearing interferometer. The elliptically figured, temperature stabilized mirror [12] focuses x-rays of 1 nm wavelength (1.24 keV) to a predetermined point. However the beam waist expands in the presence of aberrations. The use of lateral shearing interferometry to ascertain wavefront quality in coherently illuminated systems is well described [13,14]. Building on our demonstrated mirror alignment strategies [15–17], this interferometric approach offers increased sensitivity and accuracy. The optimal bending couple settings which minimize wavefront aberrations are found by applying the same linear regression analysis used to minimize surface slope error ex situ with surface slope measuring profilers [18,19]. The achieved nearly diffraction-limited focusing performance of the mirror was verified by a scanning Foucault knife-edge test.

2. Experimental system

This work was done at the test beamline (BL) 5.3.1 of the ALS. The focusing optics, shown schematically in Fig. 1, are situated inside the beamline's endstation vacuum chamber, which was carefully designed to isolate the optics from the influences of external vibrations and thermal variations [15,17]. The light transmitted by the monochromator into the chamber is incident on a 2 mm $\times$ 2 mm nano-fabricated array of slits, varying in width from 400 nm to 4 μm. This array is composed of a 100 nm thick silicon nitride window with a 2.5 μm thick gold absorbing layer onto which these features are etched by electron beam. The user-selected entrance slit serves as the optical object for the focusing mirror. Between the entrance slit and the mirror is an adjustable aperture that has the dual purpose of limiting the illumination to the clear aperture of the mirror and also as a scanning slit for initial mirror alignment. The distance between the entrance slit and the geometric center of the mirror is $r=1656$ mm. The distance to the focus from the mirror center is $r' \approx 120$ mm. This value can vary slightly as the mirror is optimized. The grazing incidence angle is $\theta=8$ mrad. Based on these parameters, the image-side numerical aperture is 2.7 mrad.

* Corresponding author. Tel.: +1 510 495 2592.
E-mail address: VVYashchuk@lbl.gov (V.V. Yashchuk).

0168-9002/$ - see front matter © 2012 Elsevier B.V. All rights reserved.
http://dx.doi.org/10.1016/j.nima.2012.10.105

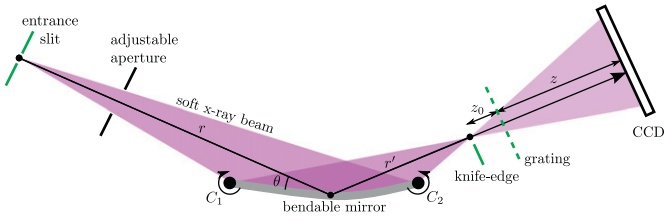

Fig. 1. Layout of optics and metrology tools in the incidence plane. The conjugate distances r and r' are from the entrance slit to the mirror center and from the mirror center to the focus, respectively. The distance from the focus to the grating along the beam is z_0, and the distance from the grating the CCD is z. The grazing incidence angle at the center of the mirror is θ.

The 102 mm long elliptically figured crystal Si mirror substrate was originally designed for a different geometry. In order to conform to the new specifications, the bending couples of the mirror (C_1 and C_2 in Fig. 1) were adjusted ex situ to set its figure closest to the desired elliptical cylinder with the ALS Long Trace Profiler (LTP) [20]. After this adjustment, the tangential slope profile of the mirror differed from the ideal elliptical slope profile by a root-mean-square (RMS) value of 0.4 μrad within the clear aperture, which spans the central 80% of the mirror length [16]. The bending couples apply torque to the mirror with the centers of rotation at the edges of the mirror, using a cantilever spring driven by a linearly translating Picomotor™ [16]. The motor positions, measured with linear variable differential transformers (LVDTs), are oriented such that positive changes cause an increased torque and consequently an increased curvature imparted to the mirror surface.

The in situ metrology tools used here are situated near the focal plane of the x-ray beam. These components – gratings, slits and knife-edges – are embedded on a single 2 mm × 2 mm nano-fabricated array, made in the same way as the object array. The gratings for shearing interferometry range in period from 4 to 8 μm. When in use, the gratings are placed a distance z_0 from the focus. The horizontal and vertical straight edges of the gold layer serve as the "knife-edge" for Foucault knife-edge testing of the beam. Accurate measurement of the beam waist requires that vibrations within the endstation vacuum chamber have amplitudes much smaller than the beam waist. We measured vibrations on the level of 10 nm or less [17] within the chamber, which is indeed much smaller than the ideal diffraction-limited beam waist. Measurements are recorded with a CCD camera placed in the path of the beam, 1.5 m downstream of the focus or a distance z from the gratings. The active area of the CCD is 0.65 cm^2, and the pixel size is 24 μm.

3. Quantitative wavefront feedback for optimal tuning of bending couples

The grating-based lateral shearing interferometer takes advantage of the Talbot effect [21] to obtain a high contrast self-image of the square wave transmission grating, seen on the CCD camera downstream. Distortion of this self-image indicates wavefront aberrations which can be recovered using well known Fourier transform based phase retrieval methods [14,22–24]. Applying this analysis results in a phase map described by

$$\phi(x) \approx \frac{2\pi}{dM}x + \frac{2\pi z}{d}\delta W'(x) \tag{1}$$

where x is the position on the CCD camera in the shear direction, d is the grating period, $M=(z+z_0)/z_0$ is the magnification of the self-image, z_0 is the distance between the focal plane and the grating, and z is the distance between the grating and the CCD camera. The Talbot effect is observed under the condition $z_0^{-1}+z^{-1}=\lambda/md^2$ for any integer m. The wavefront slope error $\delta W'(x)$ of the zeroth order beam is found by subtracting the best fitting linear ramp from the recovered phase map and scaling appropriately.

We assume a linear response of wavefront slope error to changes δC_1 and δC_2 of the mirror bending couples near the optimal configuration and apply linear regression to find the optimal settings [18,19]. The linearized model is

$$\delta W'(x) = \delta C_1 f_1(x) + \delta C_2 f_2(x) + \epsilon(x) \tag{2}$$

where f_1 and f_2 are referred to as the characteristic functions of the corresponding bending mechanisms, and ϵ is the residual error to be minimized in the least squares sense. The characteristic functions are found experimentally by applying small changes ΔC_1 and ΔC_2 to the bending couples and measuring the response

$$f_1 \approx \frac{\delta W'(x; C_1+\Delta C_1) - \delta W'(x; C_1)}{\Delta C_1} \tag{3}$$

and similarly for f_2. Using these characteristic functions and measured wavefront slope error $\delta W'(x)$, at many points $x_1, x_2, \ldots, x_N$, we find the least squares solutions to Eq. (2) for δC_1 and δC_2, denoted as δC_1^* and δC_2^*. The optimal bending couple settings are obtained by changing C_1 and C_2 by $-\delta C_1^*$ and $-\delta C_2^*$, respectively.

4. Fine alignment and tuning of a bendable focusing mirror

After the focusing mirror was configured in the ALS Optical Metrology Laboratory (OML) to match the given specifications of r, r' and θ, it was transferred to the beamline for in situ characterization and optimization. A series of recently developed at-wavelength methods [15,17,25] were used to bring the mirror near to the optimum alignment.

We then employed the shearing interferometer for finer tuning of the mirror bending couples to reduce wavefront aberrations for this particular arrangement of beamline optics. Fig. 2 illustrates a typical interference pattern (top) along with the corresponding recovered wavefront slope error map (bottom) in the plane of the CCD. The period of the grating used was 5 μm, and the self-imaging condition described above is satisfied by placing the grating at a distance $z_0 \approx d^2/\lambda = 25$ mm (for large z) from focus. The grating was translated a small amount (<1 mm) from this position along the beam in order to maximize contrast, in correspondence with this condition. The shear direction is along the horizontal axis of the images in Fig. 2. The projection of the clear aperture onto the CCD camera covers approximately the middle 80% of the observed image. All of the following analysis is done only within this clear aperture region. The precision of the measured wavefront slope error is 50 nrad, based on repeated identical measurements [17].

4.1. Correction of roll misalignment

Roll misalignment of the mirror that is a rotation of the mirror surface normal away from the nominal plane of incidence can be observed and corrected with the shearing interferometer. The top image in Fig. 3 shows the recovered wavefront slope error from an initial measurement, with a clear tilt towards the sagittal direction (perpendicular to the shear direction). This indicates a relative roll misalignment between the grating and the mirror surface. The given value for RMS is the root-mean-square wavefront slope error. We rolled the mirror into the correct alignment by minimizing the sagittal variation of wavefront slope. The result of this is the middle image in Fig. 3. The difference between these

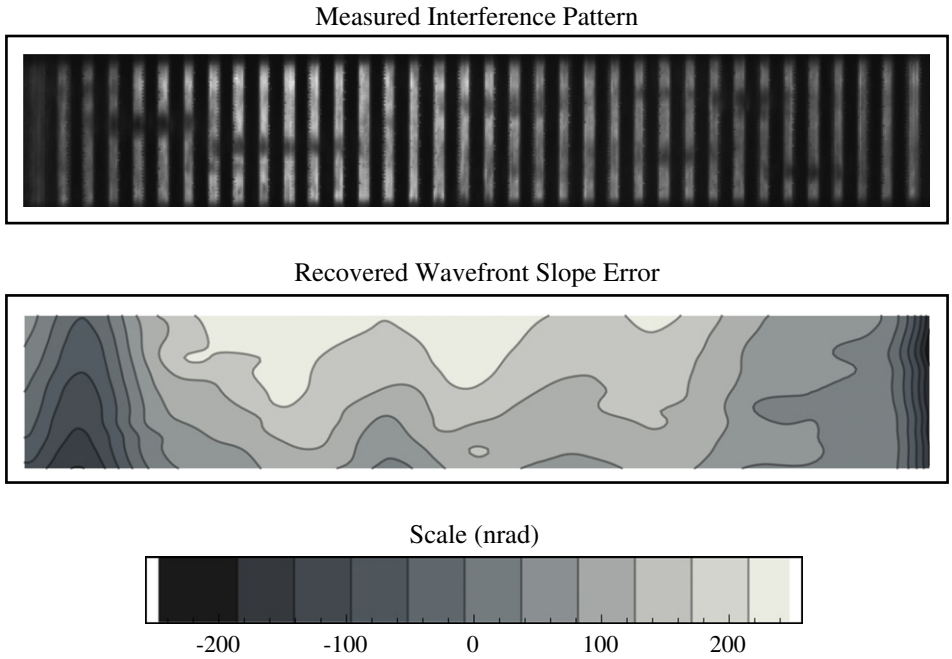

Fig. 2. Measured interference pattern (top) and the corresponding wavefront slope error (bottom) in the plane of the CCD camera. The scale shows the magnitude of variations of wavefront slope error.

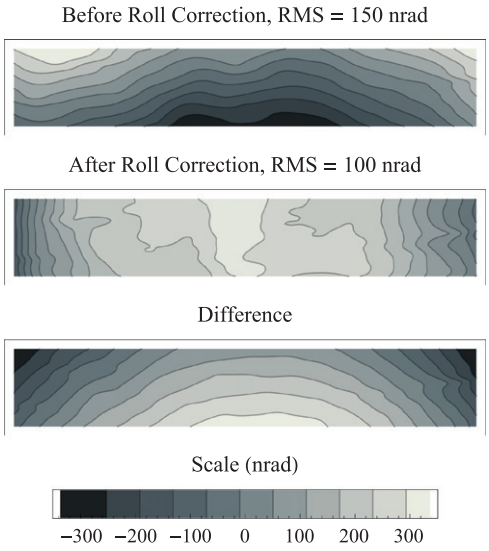

Fig. 3. Correction of roll error with shearing interferometry. An initial measurement of wavefront slope error (top) with the interferometer indicated misalignment, which was corrected resulting in the reduced wavefront slope error (middle). The difference between the two measurements is shown on bottom.

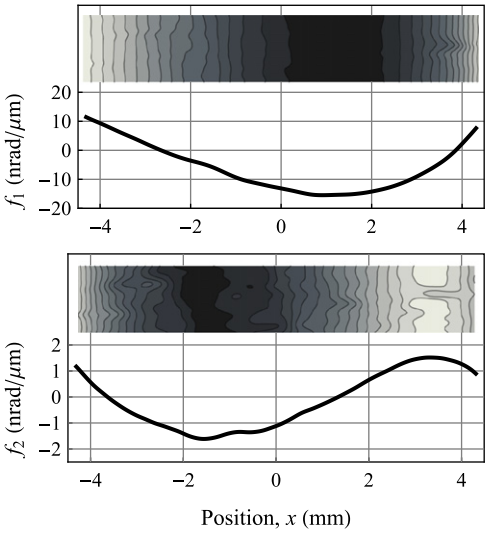

Fig. 4. Measured wavefront slope error characteristic functions (inset contours) and averaged profiles (black curves).

two measurements, at the bottom of Fig. 3, illustrates the effect of rolling the mirror about the correct alignment position, and can be used as a characteristic function of the roll mechanism for future alignment. The apparent asymmetry reflects that of the rolling mechanism.

4.2. Optimization of mirror shape

In order to optimize the settings of the mirror bending couples C_1 and C_2 we measured the characteristic functions f_1 and f_2, presented in Fig. 4. The characteristic function corresponding to bending couple C_1 was found by taking the difference of measurements before and after adjusting the motor by $\Delta C_1 = 50.0\ \mu m$. The response of wavefront slope to changes in C_2 was much weaker, because the corresponding part of the mirror surface is closer to the focus. Therefore, a larger change of $\Delta C_2 = -100.0\ \mu m$ was applied to reduce errors in the characteristic function measurement. It is important to note the high degree of linear independence between the two characteristic functions. This implies that the primary aberrations, coma and spherical aberration, can be suppressed by a suitable combination of bending couple adjustments (neglecting wavefront tilt and defocus which are not important for a single focusing mirror).

The optimal bending couple settings were found using these characteristic functions. We started with the wavefront slope error shown at the top of Fig. 5, having an RMS value of 100 nrad. From this the least squares solution to Eq. (2) was $\delta C_1^* = -11.9\ \mu m$

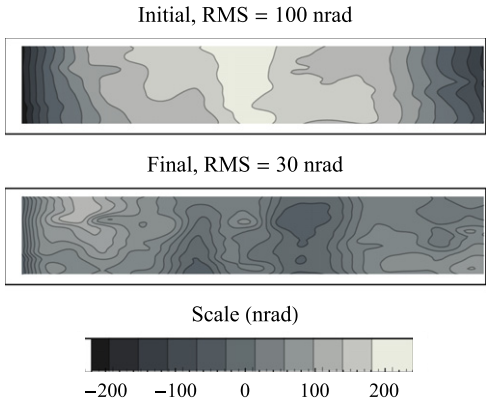

Fig. 5. Measured initial wavefront slope error (top) and wavefront slope error after optimization of bending couples (bottom).

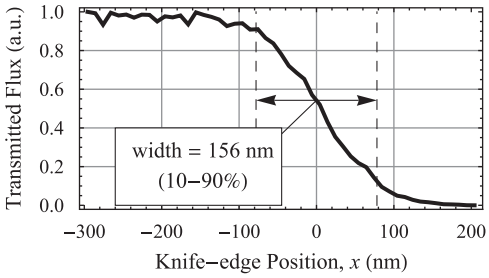

Fig. 6. Knife-edge measurement of beam width. Transmitted flux is normalized, and the x-axis is centered on the centroid of intensity.

and $\delta C_2^* = -39.2\ \mu$m, indicating that the mirror was underbent overall. After changing C_1 and C_2 by $+11.9\ \mu$m and $+39.2\ \mu$m, respectively, the resulting minimized wavefront slope error map is shown at the bottom of Fig. 5. The final RMS wavefront slope error was 30 nrad, which is at the level of measurement precision.

The resulting nearly diffraction-limited focusing performance was verified by a Foucault knife-edge test. The knife-edge was inserted into the beam in steps of 10 nm. At each step the total transmitted flux incident on the CCD camera within the region of interest was recorded as a function of knife-edge position x, as presented in Fig. 6. Background noise is subtracted from the data, and the transmitted flux is normalized such that the total beam flux is unity. The indicated width of the profile is that which spans the interval between the 10% and 90% transmitted flux points, i.e. that which encloses 80% of the beam energy. Based on this, the beam waist size is 156 nm, with a standard error of 10 nm. For comparison, in the ideal diffraction-limited scenario the width of the Airy disk (which encloses $\approx 80\%$ of the beam energy) is approximately $\lambda/2.4NA \approx 150$ nm.

5. Conclusions

We have demonstrated a new method based on shearing interferometry for in situ, at-wavelength configuration of bendable soft x-ray focusing mirrors. Using this method we aligned a single focusing mirror and optimally tuned its bending couples. This method offers higher sensitivity and more rapid assessment of wavefront aberrations, compared with previously established methods [15,17,25]. From the starting point of prealignment and presetting of the mirror with the LTP ex situ and a scanning Hartmann test in situ, we further reduced wavefront aberrations by a factor of more than 3. As a result of this combined methodology, we obtained nearly diffraction-limited one dimensional focusing of a soft x-ray beam.

It is important to note that we recently [26,27] upgraded the LTP bending couple optimization procedure to account for the beamline performance of the optic, rather than to minimize surface slope error. This upgrade improves the consistency between ex situ and in situ metrology and optimization techniques.

We are currently working to build on these promising developments in at-wavelength metrology, and to extend this methodology to Kirkpatrick–Baez mirror pairs for two dimensional focusing of soft x-ray beams. The mutual alignment of two orthogonal mirrors introduces the complication of focusing the beam with both mirrors to the same focal plane. Additionally, the effect of roll misalignments on the focusing performance is more complicated in the two dimensional case and requires more careful consideration.

A major imperative of this work is to develop tools and techniques that are based on straightforward technology and that are highly transferable. The grating-based interferometer and knife-edge test described here only require an electron-beam fabricated array of optical elements mounted on a XYZ translation stage and an x-ray CCD camera. For this reason, we strongly believe that other beamlines would be able to deploy these techniques with minimal financial or operational impact.

Acknowledgments

This work was supported by the Laboratory Directed Research and Development Program of Lawrence Berkeley National Laboratory under US Department of Energy Contract no. DE-AC02-05CH11231.

References

[1] C.M. Kewish, L. Assoufid, A.T. Macrander, J. Qian, Applied Optics 11 (2007) 2010.
[2] C.M. Kewish, M. Guizar-Sicaros, C. Liu, J. Qian, B. Shi, C. Benson, A.M. Khounsary, J. Vila-Comamala, O. Bunk, J.R. Fienup, A.T. Macrander, L. Assoufid, Optical Express 18 (2010) 23420.
[3] P. Mercere, M. Idir, P. Zeitoun, X. Levecq, G. Dovillaire, S. Bucourt, D. Douillet, K.A. Goldberg, P.P. Naulleau, S.B. Rekawa, AIP Conference Proceedings 705 (2003) 819.
[4] P. Mercere, P. Zeitoun, M. Idir, S.L. Pape, D. Douillet, X. Levecq, G. Dovillaire, S. Bucourt, K.A. Goldberg, P.P. Naulleau, S.B. Rekawa, Optics Letters 28 (2003) 1534.
[5] P. Mercere, M. Idir, T. Moreno, G. Cauchon, G. Dovillaire, X. Levecq, L. Couvet, S. Bucourt, P. Zeitoun, Optics Letters 31 (2006) 199.
[6] P. Mercere, M. Idir, T. Moreno, G. Cauchon, G. Dovillaire, X. Levecq, S. Bucourt, AIP Conference Proceedings 879 (2007) 722.
[7] H. Mimura, S. Matsuyama, H. Yumoto, H. Hara, K. Yamamura, Y. Sano, M. Shibahara, K. Endo, Y. Mori, Y. Nishino, K. Tamasaku, M. Yabashi, T. Ishikawa, K. Yamauchi, Japan Journal of Applied Physics 44 (2005) L539.

[8] H. Mimura, H. Yumoto, S. Matsuyama, Y. Sano, K. Yamamura, Y. Mori, M. Yabashi, Y. Nishino, K. Tamasaku, T. Ishikawa, K. Yamauchi, Applied Physics Letters 90 (2007) 051903.
[9] H. Mimura, S. Handa, T. Kimura, H. Yumoto, D. Yamakawa, H. Yokoyama, S. Matsuyama, K. Inagaki, K. Yamamura, Y. Sano, K. Tamasaku, Y. Nishino, M. Yabashi, T. Ishikawa, K. Yamauchi, Nature Physics 6 (2010) 146.
[10] K. Yamauchi, H. Mimura, T. Kimura, H. Yumoto, S. Handa, S. Matsuyama, K. Arima, Y. Sano, K. Yamamura, K. Inagaki, H. Nakamori, J. Kim, K. Tamasaku, Y. Nishino, M. Yabashi, T. Ishikawa, Journal of Physics: Condensed Matter 23 (2011) 394206.
[11] H. Yumoto, H. Mimura, S. Matsuyama, S. Handa, Y. Sano, M. Yabashi, Y. Nishino, K. Tamasaku, T. Ishikawa, K. Yamauchi, Review of Scientific Instruments 77 (2006) 063712.
[12] S. Yuan, M. Church, V.V. Yashchuk, K.A. Goldberg, R.S. Celestre, W.R. McKinney, J. Kirschman, G.Y. Morrison, T. Noll, T. Warwick, H. Padmore, X-Ray Optics and Instrumentation 2010 (2010) 784732.
[13] D. Malacara, Optical Shop Testing, 3rd edition, John Wiley and Sons Inc., 2007.
[14] P.P. Naulleau, K.A. Goldberg, J. Bokor, Journal of Vacuum Science and Technology B 18 (2000) 2939.
[15] S. Yuan, K.A. Goldberg, V.V. Yashchuk, R.S. Celestre, I. Mochi, J. MacDougall, G.Y. Morrison, B.V. Smith, E.E. Domning, W.R. McKinney, T. Warwick, Proceedings of SPIE 7801 (2010) 78010D.
[16] S. Yuan, K.A. Goldberg, V.V. Yashchuk, R. Celestre, W.R. McKinney, G. Morrison, J. Macdougall, I. Mochi, T. Warwick, Nuclear Instruments and Methods in Physics Research Section A: Accelerators, Spectrometers, Detectors and Associated Equipment 635 (2011) S58.
[17] D.J. Merthe, K.A. Goldberg, V.V. Yashchuk, S. Yuan, W.R. McKinney, R. Celestre, I. Mochi, J. Macdougall, G.Y. Morrison, S.B. Rakawa, E. Anderson, B.V. Smith, E.E. Domning, T. Warwick, H. Padmore, Proceedings of SPIE 8139 (2011) 813907.
[18] O. Hignette, A.K. Freund, E. Chinchio, Proceedings of SPIE 3152 (1997) 188.
[19] W.R. McKinney, J.L. Kirschman, A.A. MacDowell, T. Warwick, V.V. Yashchuk, Optical Engineering 48 (2009) 083601–083601–8.
[20] J. Kirschman, E.E. Domning, W.R. McKinney, G.Y. Morrison, B.V. Smith, V.V. Yashchuk, Proceedings of SPIE 7077 (2008) 70770A.
[21] H.F. Talbot, Philosophical Magazine 9 (1836) 401.
[22] M. Takeda, H. Ina, S. Kobayashi, Journal of Optical Society of America 72 (1982) 156.
[23] D. Malacara, Applied Optics 29 (1990) 3633.
[24] M. Servin, D. Malacara, J.L. Marroquin, Applied Optics 35 (1996) 4343.
[25] S. Yuan, V.V. Yashchuk, K.A. Goldberg, R.S. Celestre, W.R. McKinney, G.Y. Morrison, T. Warwick, H. Padmore, Nuclear Instruments and Methods in Physics Research Section A: Accelerators, Spectrometers, Detectors and Associated Equipment 649 (2011) 160.
[26] W.R. McKinney, V.V. Yashchuk, D.J. Merthe, N.A. Artemiev, K. Goldberg, Proceedings of SPIE 8501 (2012).
[27] V.V. Yashchuk, K.A. Goldberg, D.J. Merthe, N.A. Artemiev, R. Celestre, E.E. Domning, W.R. McKinney, G.Y. Morrison, M. Kunz, B.V. Smith, N. Tamura, H.A. Padmore, Experimental methods for optimal tuning and alignment of bendable mirrors for diffraction-limited soft x-ray focusing, in: Proceedings of the 11th Conference of Synchrotron Radiation Instrumentation.